RSC Advances

Hydrothermal synthesis of 2D MoS2 nanosheets for electrocatalytic hydrogen evolution reaction

Journal:	*RSC Advances*
Manuscript ID	RA-ART-09-2015-018855
Article Type:	Paper
Date Submitted by the Author:	14-Sep-2015
Complete List of Authors:	S, Murali Krishna; Jain University, Centre for Nano and Material Sciences Manjunath, Krishnappa; Jain University, Centre for Nano and Material Sciences Devaramani, Samrat; Jain University, Center for Nano and Material Sciences Reddy, Viswanth; University of Hull, Department of Chemistry T, Ramakrishnappa; Jain University, Centre for Nano and Material Sciences Nagaraju, Doddahalli; Linkoping University, IFM Department
Subject area & keyword:	

Hydrothermal synthesis of 2D MoS_2 nanosheets for electrocatalytic hydrogen evolution reaction

S. Muralikrishna,[a] K. Manjunth,[a] D. Samrat,[a] Viswanath Reddy,[c] T. Ramakrishnappa*[a,b] D. H. Nagaraju[d]

[a]Centre for Nano and Material Sciences, Jain University, Jakkasandra, India.
[b]Dayananda Sagar Academy of Technology and Management, Udayapura, Opp Art of Living, Kanakapura Road, Bangalore-560082
[c]Liquid crystal research group, Department of Chemistry, University of Hull, Cottingham Road, Hull HU6 7RX.
[d]King Abdullah University of Science and Technology, Thuwal, Saudi Arabia.

*To whom correspondence should be addressed. Dr. Ramakrishnappa. T, Mobile +91-9035925504, Direct Tel: +91-80-27506270: Email:swadheshi26@gmail.com

Abstract

Nanostructured molybdenum disulfide (MoS_2) is a most promising catalyst to produce molecular hydrogen by electrochemical method. Herein, we have designed and synthesized highly electocatalytic active 2D MoS_2 nanosheets (NS) from molybdenum trioxide (MoO_3) by facile hydrothermal method and compared their electrocatalytic activities for hydrogen evolution reaction (HER). The electrochemical characterization was performed using linear sweep voltammetry (LSV) in acidic medium. MoS_2 NS shows HER onset potential at about 80 mV *vs* reversible hydrogen electrode (RHE) which is much lower than the MoO_3 (300 mV). The MoS_2 NS and MoO_3 show a current density of 25 mA/cm^2 and 0.3 mA/cm^2, respectively at a overpotential of 280 mV *vs* RHE. The MoS_2 NS showed 83 times higher current density when compared to the MoO_3. Tafel slope of MoS_2 NS and MoO_3 is about 90 mV/dec and 110 mV/dec respectively. This suggesting that MoS_2 NS is a better electrocatalyst when compared to MoO_3 and follows Volmer-Heyrovsky mechanism for HER.

Introduction

The global energy demand is continuously growing due to the remarkable issues of fossil fuels depletion and CO_2 secretion.[1-3] To solve these two issues molecular hydrogen is considered as an alternative green energy fuel.[4] The numerous methods are available for the production of molecular hydrogen.[5] Presently, the hydrogen is generated by steam reformation process of methane for many industrial applications. However, in this method the combustion of methane gas releases enormous amount of carbon dioxide which leads to adverse climate change.[6-7] The green route for the production of hydrogen is either by electrochemical or (photo)electrochemical process.[8-9] These two methods require highly efficient catalyst to realize the commercial applications. The noble metal platinum is considered as the best catalyst for hydrogen evolution reaction.[10] However, the platinum metal is low earth abundant and expensive.[11] Hence, the present challenge is to design and synthesis of nonprecious and earth abundant metal for hydrogen evolution reaction that can produce hydrogen under low overpotential and catalytically stable for longer cycles.[12-13] Different nanostructured catalysts such as metal sulfides, metal carbides, metal nitrides, metal phosphides, metal selenides, metal borides, metal nanoparticles, metal alloys and molecular catalysts have been introduced to produce molecular hydrogen.[7, 14-22]

Recently, two dimensional layered materials such as graphene and transition metal chalcogenides, has created tremendous interest due to its unique physical and chemical properties.[23-24] Amongst the different types of layered materials, MoS_2 is special due to its interesting electric and magnetic properties[24] as well as numerous potential applications such as Photo(electro)catalysts, energy storage devices, photoluminescence, sensors and so on.[25-28] Now a days, it has received great attention for HER catalyst due to its high catalytic activity, high chemical stability, low cost and ease of synthesis.[29] Theoretical calculations by DFT as well as experiments[30-32] confirms that the electrocatalytic activity of MoS_2 mainly depends on

the co-ordinated sulphur edge sites rather than the basal plane.[33] Bulk MoS_2, which contains number of single layer MoS_2 NS and these layers are staked through weak Van der walls force of interactions and arranged in a hexagonal closed pack fashion.[34] It is reported that bulk MoS_2 shows poor catalytic activity for the practical applications.[10] For this reason, different strategies have been developed to enhance the electrical conductivity. Mainly, conversion of bulk into nanosized and exposing the active sites by altering the nanostructures. Incorporating of conductive materials such as promoters, carbon substrates, metal oxide, metal sulfide and defects on the surface layers.[35-46] For example, Hu *et al.* reported series of MoS_x (x=2 or 3) thin films and incorporating promoters such as Co, Ni and Fe for HER.[6,11,13-15] Jaramillo *et al.* reported the various MoS_2 nanostructures for HER.[34,39-41] Lou *et al.* reported MnS@MoS_2 core–shell microcubes, MoS_2 nanosheets supported on N-doped carbon nanoboxes, MoS_2 carbon one-dimensional nanostructures, defect rich MoS_2 ultrathin nanosheets for lithium storage and electrocatalytic applications.[42,43,47-50] Jin *et al.* developed chemically exfoliated metallic MoS_2 nanosheets for HER[51] Chen *et al.* reported MoO_2 nanobelts@nitrogen self-doped MoS_2 nanosheets, porous metallic MoO_2-supported MoS_2 nanosheets and Pt nanoparticles/MoS_2 nanosheets/carbon fibers for HER.[44-46,52] Sampath *et al.* reported few-layer alloys of $MoS_{2(1-x)}Se_{2x}$ for HER.[53]

Here, we have designed and synthesized 2D MoS_2 nanosheets (NS) from molybdenum trioxide (MoO_3) by facile hydrothermal method. We have used molybdenum trioxide (MoO_3) as precursor instead of ammonium heptamolybate tetrahydrate for altering the morphology and enhancing the catalytic active sites of the MoS_2 catalyst. The synthesized MoS_2 NS having more defects at the edges as confirmed by high resolution transmission electron microscopy (HRTEM) images and XRD analysis. These materials were further used as an electrocatalyst for HER in acidic medium. The MoS_2 NS and MoO_3 show onset potential at about 80 mv and 300 mv *vs* reversible hydrogen electrode (RHE) respectively. The MoO_3

and MoS_2 NS show a current density of 0.3 mA/cm^2 and 25 mA/cm^2, respectively at a overpotential of 280 mV *vs* RHE. The MoS_2 NS showed positive onset potential and 83 times higher current density as compared to MoO_3 and also commercial MoS_2 (C-MoS_2). The Tafel slope of MoO_3, C-MoS_2 and MoS_2 NS electrode showed 110, 107 and 90 mV/dec, respectively. The lower Tafel slope of MoS_2 NS electrode indicates that it acts as a better electrocatalyst when compared to MoO_3 and C-MoS_2 electrodes. Tafel slope of MoS_2 NS suggest that Heyrovsky step is the rate determining step (RDS)[10, 54-55] and HER takes place according to the Volmer-Heyrovsky mechanism. The prepared electrode is catalytically stable for longer cycles. The observed onset potential and overpotential are almost equal to that of previously reported single-layer MoS_2 coating on carbon nanotubes[56] and higher current density and lower Tafel slope as compared to mechanical activated MoS_2.[57]

Instrumentation

All electrochemical measurements were performed using a CHI660D potentiostat (CH instruments, Austin, USA). Powder X-ray diffraction data was recorded using Philips X'pert PRO PANalytical X-ray diffractometer with graphite monochromotaized Cu-Kα (1.5418 A^o) radiation. Scanning electron microscopy was carried out using FEI (Nova nano). A JEOL3000F Transmission Electron Microscope (300kV accelerating voltage) was used for generating images of MoO_3 and MoS_2.

Materials and reagents

All the chemical reagents were used as received without any further purification. Deionised water was used in all the experiments. Ammonium heptamolybate tetrahydrate (≥99%), Thiourea (99-101%), isopropanol (99.7%), sulphuric acid (95-98%) and ethanol (99.9%) were purchased from the Merck. Nafion solution (5%) was purchased from sigma Aldrich.

Synthesis of Molybdenum trioxide (MoO_3)

Molybdenum trioxide was prepared by heating 0.5 g of Ammonium heptamolybate tetrahydrate at 450 ^oC for 2 h in presence of atmospheric air.

Synthesis of Molybdenum sulpfide nanosheets (MoS_2 NS)

MoS_2 NS were synthesized by mixing 0.0575 g of MoO_3 and 0.1332 g of thiourea in 40 mL water. The reaction mixture was a stirred for 0.5 h then transferred in to 50 mL Teflon lined autoclave and kept in furnace at 200 ^oC for 24 h. After the completion of reaction the autoclave was cooled naturally and the black precipitate was separated by centrifugation and washed several times with water and ethanol. The washed precipitate was dried at 60 ^oC for 12 h.

Electrochemical measurements

Before electrode modification, the glassy carbon (GC, 3 mm diameter) electrode was polished with alumina slurry of three different particle size (1, 0.3 and 0.05 micron) followed by rinsing with copious amount of distilled water. Then the electrodes were sonicated in ethanol-water (1:1) mixture for about 5 min, followed by rinsed with ample quantity of distilled water and dried naturally at room temperature.

4 mg of MoS_2 NS was dissolved in 1 mL of water-isopropanol mixture (0.7:0.3 ratio) and sonicated for 30 min. 10 µL of that solution was drop casted on the surface of glassy carbon electrode and dried under room temperature. The HER activity was measured at 25 ^oC in 0.5 M H_2SO_4 (pH=0.8) with a standard three electrode system containing MoS_2 modified glassy carbon electrode as a working electrode, platinum wire as a counter electrode and Ag/AgCl (1 M KCl) as a reference electrode. Prior to electrochemical measurement 0.5 M H_2SO_4 is saturated with high purity hydrogen gas and it was calibrated with respect to standard reversible hydrogen electrode (RHE) with Pt as working electrode and Pt wire as counter electrode.[58] All electrode potentials are represented with respect to RHE according to

equation E (RHE) = E (Ag/AgCl)+0.230 V. Linear sweep voltammetry was performed to measure electrocatalytic HER results with a scan rate of 1 mV/s in 0.5 M H_2SO_4 electrolyte solution.

Results and discussion

The schematic representation of the synthesis of MoO_3 and MoS_2 NS is shown in scheme 1. Ammonium heptamolybate tetrahydrate heated at 450 ^oC in presence of air, decomposition takes place to give MoO_3 particles. Mo(VI) present in MoO_3 reduces into Mo(IV) when hydrothermally treated at 200 ^oC in presence of excess of thiourea. The excess of thiourea acts both as reducing agent to reduce Mo(VI) into Mo(IV) as well as efficient additive to stabilize the defect-rich nanosheet morphology.[47] The reduced Mo(IV) reacted with excess of thiourea to nucleate and grow into MoS_2 nanoparticles and finally these particles are grown into defect-rich 2D nanosheets.[47,59] The ammonia present in the reaction mixture prevents the stacking of MoS_2 NS and hence the formation of thin MoS_2 NS.[60]

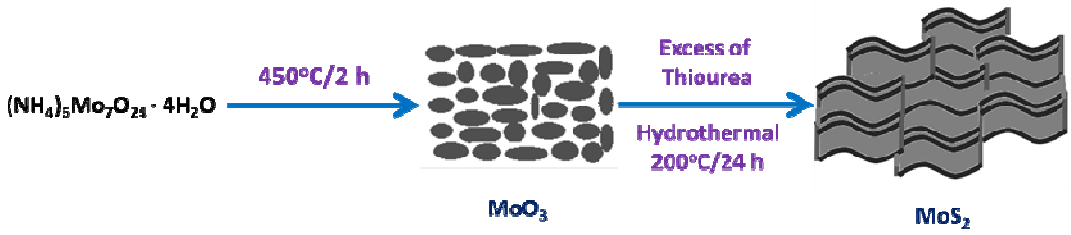

Scheme 1. Schematic representation for synthesis of MoO_3 and MoS_2.

XRD studies

The XRD pattern obtained from as-prepared MoO_3 and MoS_2 NS are shown in Figure. 1. The diffraction peaks for MoO_3 NP corresponding to the orthorhombic phase (JCPDS card No: 5-506) with the space group Pbnm (No-62) and the lattice parameters a=3.966 Å, b=13.88 Å, c=3.703 Å. The lattice faces of MoO_3 NP are (210), (022), (112), (270), (202), (222), (301), (063) are parallel to the highest intense peak plane (040) are co-related to the typical peaks obtained in diffraction pattern.

The diffraction pattern for MoS_2 refers to a hexagonal structure (JCPDS card No: 75-1539) with the space group P63/mnc (No-194) and the lattice constants were estimated as a=3.14 Å and c=12.53 Å. The lattice faces of MoS_2 are (002), (100), (103), (110). The peak of (002) plane shifts to a smaller angle indicating that there is an expansion towards (001) direction. The interlayer spacing (002) of as prepared MoS_2 was found to be 6.36Å, which is larger compared to bulk MoS_2 (6.1554 Å).[61] The broadening of XRD planes such as (100) and (110) indicates that as prepared MoS_2 contains large number of defects.[47] The difference in the d space (002) causes a uniaxial tensile strain along [001] direction in the as-prepared MoS_2.

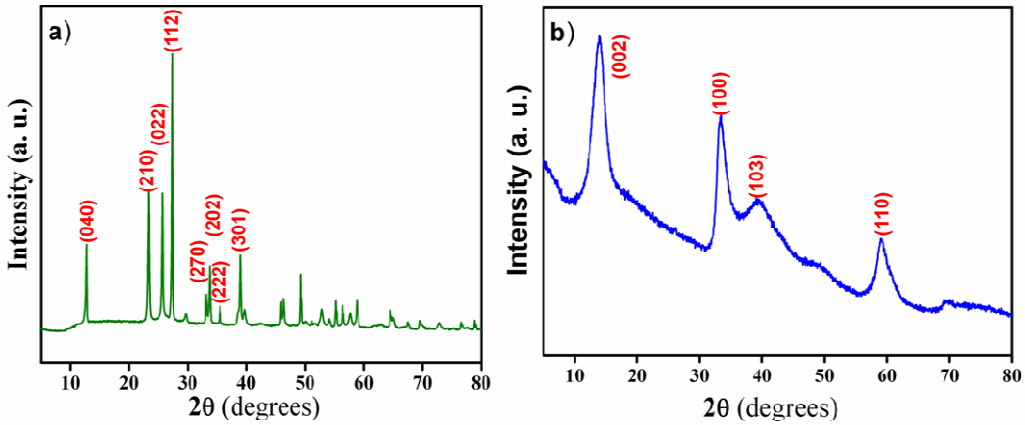

Figure.1 XRD pattern of a) MoO_3 and b) MoS_2

Surface morphology studies

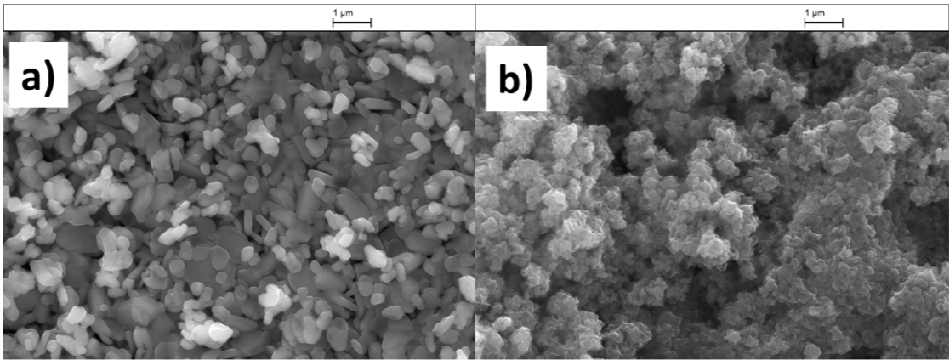

Figure. 2. SEM image of a) MoO_3 and b) MoS_2

Scanning electron microscopy (SEM) analysis has been carried out to study the surface morphology of the as synthesized MoO_3 and MoS_2 as shown in Figure. 2. MoO_3 shows the particle like morphology. These MoO_3 was simultaneously sulphurized to form MoS_2 by hydrothermal process using excess thiourea. SEM image of MoS_2 reveal that homogeneous arrangement of MoS_2 clusters (Figure. 2b).

We have further investigated the morphology by using transmission electron microscopy (TEM) as shown in Figure. 3. The TEM images of MoO_3 indicate that typical nanoparticles presented on the surface grids (Figure. 3a). The diameter of these nanoparticles have been estimated to be around 100-200 nm. MoS_2 images show typical sheets like morphology and having many thin nano-sheets (Figure. 3b). The HRTEM images of the MoS_2 nanosheets clearly display, the obtained material consists of ultrathin nanosheets, which was also confirmed from XRD pattern. The d-spacings on the surface and edges of the MoS_2 nanosheets are briefly explained using HRTEM, the images are clearly predicted in the figure 3c and 3d. The various d-spacings such as 0.27 nm, 0.22 nm and 0.15 nm are observed on the basal plane of the hexagonal MoS_2 nanosheets which are assigned to a single (100) plane. These interpalnar spacings and individual planes are perfectly coincidence with d-spacings of XRD pattern. In addition, we have observed various breakdowns and deformations on the surface of nanosheets. This indicates, the obtained material has large number of defects. Furthermore, we have found an important issue on the surface of nanosheet is the individual planes (100) are spread in different directions of the nanosheets indicates the unusual arrangement of atoms, resulting breakdown of basal planes and leads to the formation of new edges. In contrast, an interesting structure was observed at the curled edge of the nanosheets with the d-space of 6.2 Å, which is clearly shown in HRTEM image of figure 3d. In addition, we noticed large number of defects find at the curled edge (shown in

circle in Figure 3d). These defects leads to broadening of XRD peaks such as (100) and (110) planes.

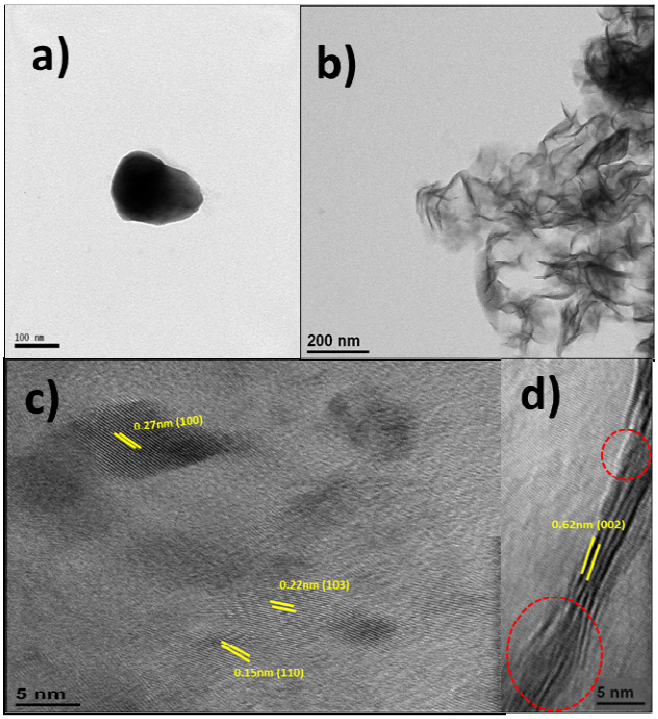

Figure. 3. TEM images of a) MoO_3, b) MoS_2 NS. c) and d) are HRTEM images of MoS_2 NS.

Electrochemical studies

Linear sweep voltammetry studies

The electrocatalytic activity of MoS_2 NS modified GC electrode was investigated by LSV using three electrode configuration in 0.5 M H_2SO_4 at room temperature as shown in Figure. 4a. The MoS_2 NS modified electrode showed an onset potential of 80 mV *vs* RHE. The observed onset potential and overpotential are almost equal to that of previously reported single-layer MoS_2 coating on carbon nanotubes[56] and higher current density as compared to mechanical activated MoS_2.[57] We have compared the electrocatalytic activity of MoS_2 with MoO_3, C-MoS_2, Pt and bare GC electrodes (Figure 4). The MoO_3 and C-MoS_2 modified electrode showed 0.3 mA/cm^2 at overpotential of 280 mV *vs* RHE. The MoS_2 NS electrode

exhibited positive onset potential and 83 times higher current density as compared to MoO_3 and C-MoS_2 electrodes. The observed current density of MoS_2 NS electrode was compared with the previous reports listed in Table. 1.

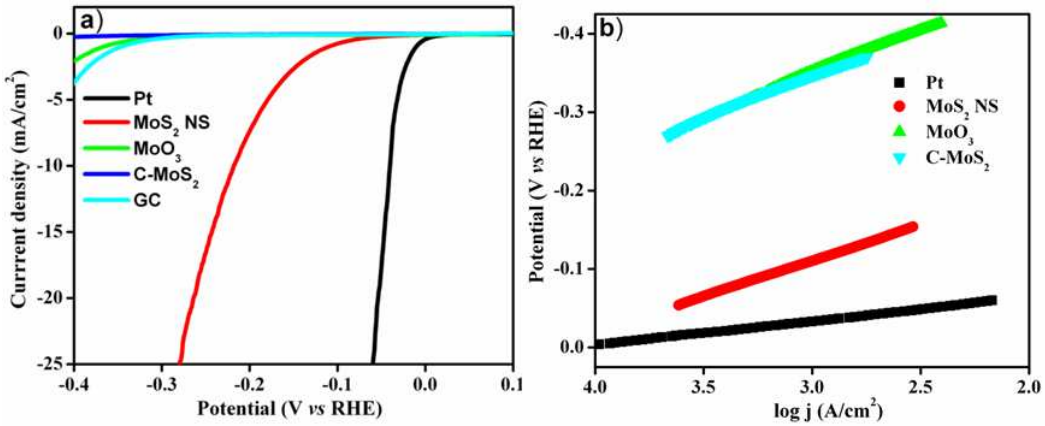

Figure. 4 a) LSVs of GC, MoO_3, C-MoS_2, MoS_2 NS and Pt electrodes measured in 0.5 M H_2SO_4. b) Tafel plots for various electrodes in 0.5 M H_2SO_4.

HER mechanism

The presently accepted mechanism for HER according to the fallowing three steps.

(1) Volmer: $H_3O^+ + M(e-) \longrightarrow MH_{ads} + H_2O$

(2) Heyrovsky: $H_3O^+ + MH_{ads} + M\ (e-) \longrightarrow 2M + H_2O + H_2$

(3) Tafel: $2MH_{ads} \longrightarrow 2M + H_2$

Where, M represents an empty metal active site and MH_{ads} represents an adsorbed H intermediate. The HER takes place according to the two step reaction process. The first step is called Volmer or discharge step. In this step, hydrogen atom adsorbed on the electrode surface results from an electron coupled with proton present in an acidic electrolyte. In the second step the molecular hydrogen evolved either by Heyrovsky or Tafel step. If the molecular hydrogen evolved from the coupling of adsorbed hydrogen with transfer of another proton, that is called Heyrovsky step or If the molecular hydrogen evolved from the coupling of two adsorbed hydrogen atoms on the electrode surface, that is called Tafel step. Therfore the HER takes place either by Volmer-Heyrovsky or Volmer-Tafel reaction.[36] In both the

cases, the overall reaction rate depends on the Gibbs free energy of hydrogen atom adsorption (ΔG_H^o) due to H_{ads} always involved in the reaction process. If the H atom adsorbed on the empty active site of the electrode surface too srongly, the discharge step (Heyrovsky or Tafel step) becomes difficult. If the H atom adsorbed on the empty active site of the electrode surface too weekly, the adsorption step (Volmer step) is difficult that limits in the overall turnover rate. Therefore, an optimal HER catalyst should bind H atom moderately and exhibits ΔG_H^o almost zero.[35,71-73] Tafel plots are commonly used to investigate HER mechanism and the electrocatalytic activity. If the Tafel slope is closer to 120 mV/dec, the HER mechanism takes place via combination of Volmer-Heyrovsky steps or if the slope is nearly 30 mV/dec, the HER mechanism follows combination of Volmer-Tafel steps.[10,54-55] In other words, smaller the Tafel slope indicates the faster reaction rates with increasing the potential.[74]

The Tafel plots constructed for different electrodes in the present investigation are shown in Figure. 4b. We have fitted the linear portions under different overpotential region for the comparison. The Tafel slope was found to be 90 mV/dec for MoS_2 NS electrode and 32 mV/dec for Pt electrode. This indicates that Tafel step is RDS and HER takes place according to the Volmer-Tafel steps on the surface of Pt electrode while for the MoS_2 NS electrode Heyrovsky step is the RDS and fallows Volmer-Heyrovsky mechanism.[10,54-55] The observed Tafel slope is lesser than that of the previously reported mechanical activated MoS_2, MoS_2 sheet, MoS_2 sphere, MoS_2 and $MoSe_2$ films and MoS_2 particles.[31,57,74-75] The MoO_3 NP and C-MoS_2 electrodes shows a Tafel slope of 110 mV/dec and 108 mV/dec respectively. The observed Tafel slope for MoO_3 NP and C-MoS_2 electrodes are higher as compared to the MoS_2 NS electrode. This indicates that MoS_2 NS electrode shown good electrocatalytic activity towards HER.

Table. 1 Electrochemical HER comparison of previously reported catalysts.

Catalyst	Loading (mg cm^{-2})	Electrolyte	Overpotential (mV)	Current density (mA cm^{-2})	Tafel slope (mV/dec)	Reference
Mo1Soy/rGO	-	0.1 M $HClO_4$	177/RHE	10	62.7	12
Amorphous molybdenum sulfide	-	0.5 M H_2SO_4	200/RHE	10	53	41
Defect-rich MoS2 ultrathin nano sheets	0.285	0.5 M H_2SO_4	300/RHE	70.5	50	47
Metallic MoS_2 NS	-	0.5 M H_2SO_4	187/RHE	10	43	51
Single layer MoS_2 coating on carbon nanotubes	-	0.1 M H_2SO_4	236/RHE	10	63	56
MoS_2 on Au electrode	0.00103	0.5 M H_2SO_4	150/SHE	0.92	69	62
Amorphous MoS_3	0.2	1.0 M H_2SO_4	170/RHE	20	-	63
MoS_2 /Mesoporous graphene foam	0.21	0.5 M H_2SO_4	200/RHE	100	42	64
MoS_2/RGO	0.285	0.5 M H_2SO_4	150/RHE	9	41	65
Amorphous carbon supported MoS_2 NS	-	0.5 M H_2SO_4	200/RHE	91	40	66
Oxygenated MoS_2 NS	0.285	0.5 M H_2SO_4	300/RHE	126.5	55	67
WS_2/rGO	0.4		300/RHE	23		68
Li-MoS_2 Nanoparticles	-	0.5 M H_2SO_4	200/RHE	200	62	69
WS_2 NS	0.285	0.5 M H_2SO_4	150/RHE	9.66	72	70
MoS_2 NS	0.566	0.5 M H_2SO_4	280/RHE	25	90	This Work

Electrochemical impedance spectroscopy

The electrocatalytic activities of MoS_2 NS, C-MoS_2 and MoO_3 were further examined with the help of electrochemical impedance spectroscopy (EIS). EIS is useful technique to characterize interface reactions and electrode kinetics in HER. Fig 5a. shows the Nyquist plots recorded for all the three above mentioned materials at an over potential of 150 mV vs RHE, where x-axis and y-axis represent the real and imaginary parts of impedance respectively. Charge transfer resistance (R_{ct}) for all the three materials were understood from the semicircles observed in the EIS spectra. Among the three, MoS_2 NS exhibited the semicircle with smallest diameter. This indicates the R_{ct} of HER in the case of MoS_2 NS is the smallest among the three materials at the investigated potential.[64,76-77] Hence, the faster reaction rate is achieved with MoS_2 NS electrode.

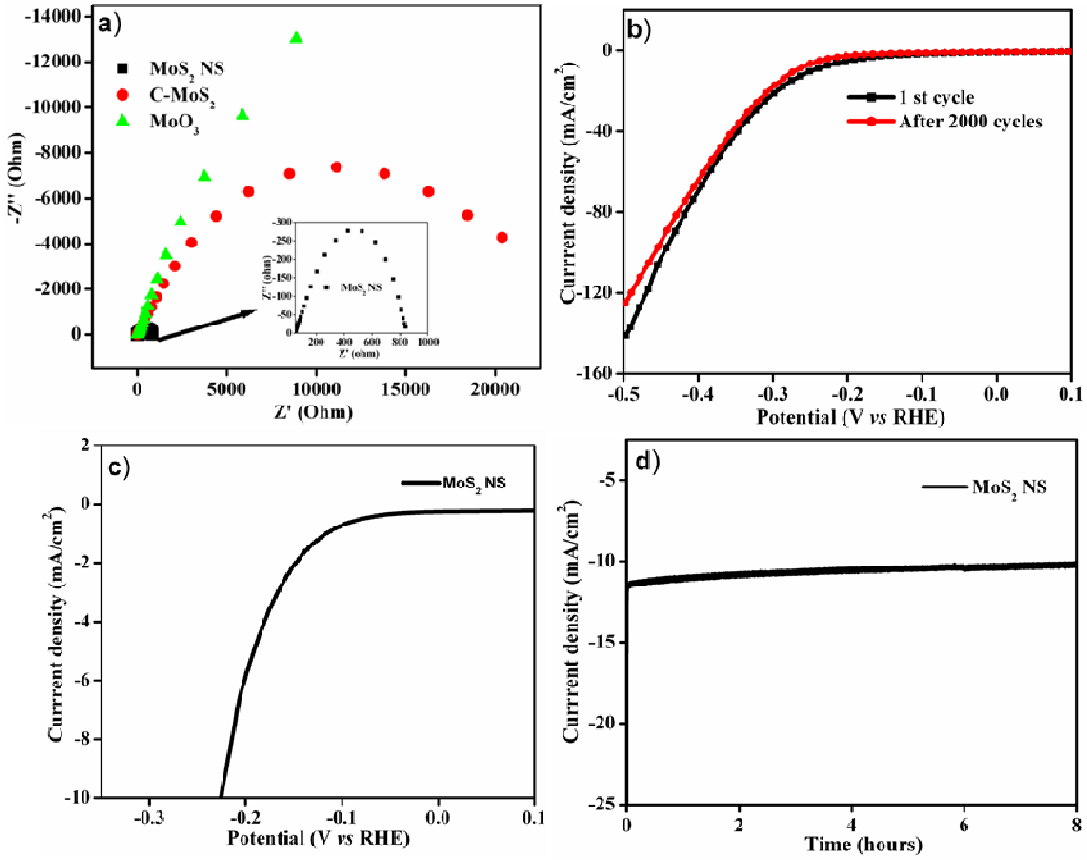

Figure 5. a) Nyqist plots recorded for MoS_2 NS C-MoS_2 and MoO_3 electrodes in 0.5 M H_2SO_4 at the applied potential of 150 mV *vs* RHE. b) HER stability of MoS_2 NS electrode before and after 2000 cycles in 0.5 M H_2SO_4. c) LSV of MoS_2 NS electrode

recorded after 2000 cycles with scan rate 5 mV/s. d) Chronoamperometric response of MoS_2 NS electrode in 0.5 M H_2SO_4 at the applied potential of 200 mV *vs* RHE.

Stability is one of the most important factor used to evaluate a performance of good catalyst. The stability of the MoS_2 NS electrode towards HER has been tested by repeated cycling at scan rate of 100 mV/s as shown in Figure. 5b. The slight decrease in currents due to hydrogen evolution was observed after 2000 cycles. We also provided the graph of current density at 10 mA/cm^2 recorded after continuous cycles of MoS_2 NS electrode at a scan rate of 5 mV/s shown in Figure. 5c. Further, chronoamperometric technique was used to analyse the long-term stability of MoS_2 NS electrode at an overpotential of 200 mV *vs* RHE. Figure. 5d. represents a plot of current density *vs* time recorded using MoS_2 NS electrode. The negligible decrease in current density after 8 h was observed. These studies demonstrates that the prepared catalyst is quite stable for long cycling.

Conclusion

In summary, we have synthesized MoS_2 NS for electrocatalytic HER. The electrode showed low onset potential (80 mV *vs* RHE) for HER and attained current density of 25 mA/cm^2 at a overpotential 280 mV *vs* RHE. The observed current density is higher than the previously reported MoS_2 catalysts at same overpotential region. A Tafel slope of 90 mV/dec suggested that Heyrovsky step is the RDS and hence HER taking place according to Volmer-Heyrovsky mechanism. In addition, prepared electrode shows good catalytic stability for longer cycles.

Acknowledgments

The authors thanks to Jain University, DST-SERB and DST Nanomission for financial support. We also wish to extend our gratitude to Dr Narayanappa Sivasankar, Riogen, Inc. catalysis for chemical and energy, South Jersey Technology Park, Mullica Hill, NJ 08062, USA 08852, for pre-review of the manuscript.

References

1 N. S. Lewis, D. G. Nocera, *Proc. Natl. Acad. Sci. U. S. A.,* 2006, **103**, 15729-15735.

2 Climate Change 2007: Synthesis Report. Contribution of Working Groups I, II and III to the Fourth Assessment. Report of the Intergovernmental Panel on Climate Change, ed. R. Pachauri and A. Reisinger, IPCC, Geneva, 2008.

3 M. S. Dresselhaus, I. L. Thomas, *Nature,* 2001, **414**, 332-337.

4 G. Ajayakumar, M. Kobayashi, S. Masaoka, K. Sakai, *Dalton. Trans.,* 2011, **40**, 3955-3966.

5 N. Bundaleska, D. Tsyganov, R. Saavedra, E. Tatarova, F. M. Dias, C. M. Ferreira. *Int. J. Hydrogen. Energy.* 2013, **38**, 9145-9157.

6 D. Merki, X. Hu, *Energy Environ. Sci.,* 2011, **4**, 3878-3888.

7 W. F. Chen, J. T. Muckerman, E. Fujita, *Chem. Commun.,* 2013, **49**, 8896-8909.

8 M. G. Walter, E. L. Warren, J. R. McKone, S. W. Boettcher, Q. Mi, E. A. Santori, N. S. Lewis, *Chem. Rev.,* 2010, **110**, 6446-73.

9 J. A. Turner, *Science,* 2004, **305**, 972-74.

10 S. Sarkar, S. Sampath, Chem. Commun., 2014, **50**, 7359-7362.

11 D. Merki, H. Vrubel, L. Rovelli, S. Fierro, X. Hu, *Chem. Sci.,* 2012, **3**, 2515-2525.

12 W. F. Chen, S. Iyer, S. Iyer, K. Sasaki, C. H. Wang, Y. Zhu, J. T. Muckerman, Etsuko Fujita, *Energy Environ. Sci.,* 2013, 6, 1818-1826.

13 C. G. M-Guio, X. Hu, *Acc. Chem. Res.,* 2014**, 47**, 2671-2681.

14 D. Merki, X. Hu*, Energy. Environ. Sci.* 2011, **4**, 3878-3888.

15 H. Vrubel, D. Merki, X. Hu, *Energy. Environ. Sci.* 2012, **5**, 6136-6144.

16 E. J. Popczun, J. R. McKone, C. G. Read, A. J. Biacchi, A. M. Wiltrout, N. S. Lewis, R. E. Schaak, *J. Am. Chem. Soc.,* 2013, **135**, 9267-9270.

17 D. Kong, H. Wang, J. J. Cha, M. Pasta, K. J. Koski, J. Yao, Y. Cui, *Nano Lett.,* 2013, **13**,

1341-1347.

18 H. Wang, D. Kong, P. Johanes, J. J. Cha, G. Zheng, K. Yan, N. Liu, Y. Cui, *Nano Lett.,* 2013, **13**, 3426-3433.

19 H. Vrubel and X. Hu, *Angew. Chem.,* 2012, **124**, 12875.

20 B. Kumar, S. Saha, M. Basu, A. K. Ganguli, *J. Mater. Chem. A.* 2013, **1**, 4728-4735.

21 C. Cui, M. Ahmadi, F. Behafarid, L. Gan, M. Neumann, M. Heggen, B. R. Cuenya, P. Strasser, *Faraday Discuss,* 2013, **162**, 91-112.

22 V. S. Thoi, Y. Sun, J. R. Long, C. J. Chang, *Chem. Soc. Rev.* 2013, **42**, 2388-2400.

23 X. Huang, Z. Zeng, S. Bao, M. Wang, X. Qi, Z. Fan, H. Zhang, *Nature Communications*, 2013, **4**, 1-8.

24 C.N.R. Rao, U. Maitra, U. V. Waghmare, *Chemical Physics Letters*, 2014, **609**, 172-183.

25 U. Maitra, U. Gupta, M. De, R. Datta, A. Govindaraj, C. N. R. Rao, *Angew. Chem. Int. Ed*. 2013, **52**, 13057-1306.

26 C. N. R. Rao, K. Gopalakrishnan, U. Maitra, *ACS Appl. Mater. Interfaces*, 2015, **7**, 7809-7832.

27 M. Chen, X. Yin, M. V. Reddy, S. Adams, *J. Mater. Chem. A*, 2015, **3**, 10698-10702.

28 G. Eda, H. Yamaguchi, D. Voiry, T. Fujita, M. Chen, M. Chhowalla, *Nano Lett*., 2011, **11**, 5111-5116.

29 Z. Wu, B. Fang, Z. Wang, C. Wang, Z. Liu, F.Liu, W. Wang, A. Alfantazi, D. Wang, D. P. Wilkinson, *ACS Catal*. 2013, **3**, 2101-2107.

30 B. Hinnemann, P. G. Moses, J. Bonde, K. P. Jørgensen, J. H. Nielsen, S. Horch, I. Chorkendorff, J. K. Nørskov, *J. Am. Chem. Soc.,* 2005, **127**, 5308-5309.

31 J. Bonde, P. G. Moses, T. F. Jaramillo, J. K. Norskov, I. Chorkendorff, *Faraday Discussions,* 2008, **140**, 219-231.

32 H. I. Karunadasa, E. Montalvo, Y. Sun, M. Majda, J. R. Long, C. J. Chang, *Science*

2012, **335**, 698-702.

33 L. Liao , J. Zhu , X. Bian , L. Zhu , M. D. Scanlon , H. H. Girault, B. Liu, *Adv. Funct. Mater.* 2013, **23**, 5326-5333.

34 T. F. Jaramillo, K. P. Jørgensen, J. Bonde, J. H. Nielsen, S. Horchm I. Chorkendorff, *Science*, 2007, **317**, 100-102.

35 A. B. Laursen, S. Kegnas, S. Dahla, I. Chorkendorff, *Energy Environ. Sci.,* 2012, **5**, 5577-5591.

36 C. G. M-Guio, L-A. Stern, X. Hu, *Chem. Soc. Rev.,* 2014, **43**, 6555-6569.

37 Y. Yan, B.Y. Xia, Z. Xu, X. Wang, *ACS Catal*. 2014, **4**, 1693-1705.

38 P. C. K. Vesborg, B. Seger, I. Chorkendorff, *J. Phys. Chem. Lett.* 2015, **6**, 951-957.

39 Z. Chen, D. Cummins, B. N. Reinecke, E. Clark, M. K. Sunkara, T. F. Jaramillo, *Nano Lett*., 2011, **11**, 4168-4175.

40 J. Kibsgaard, Z. B. Chen, B. N. Reinecke and T. F. Jaramillo, *Nat. Mater*., 2012, **11**, 963–969.

41 J. D. Benck, Z. B. Chen, L. Y. Kuritzky, A. J. Forman, T. F. Jaramillo, *ACS Catal*., 2012, **2**, 1916-1923.

42 B. Y. Xia, Y. Yan, X. Wang, X. W. Lou, *Mater. Horiz.,* 2014, **1**, 379-399.

43 L. Zhang, H. B. Wu, Y. Yan, X. Wang, X. W. Lou, *Energy Environ. Sci.,* 2014, **7**, 3302-3306.

44 W. Zhou, D. Hou, Y. Sang, S. Yao, J. Zhou, G. Li, L. Li, H. Liu, S. Chen, *J. Mater. Chem. A,* 2014, **2**, 11358-11364.

45 L. Yang, W. Zhou, D. Hou, K. Zhou, G. Li, Z. Tang, L. Lia, S. Chen, *Nanoscale,* 2015, **7**, 5203-5208.

46 W. Zhou, K. Zhou, D. Hou, X. Liu, G. Li, Y. Sang, H. Liu, L. Li, S. Chen, *ACS Appl. Mater. Interfaces,* 2014, **6**, 21534-21540.

47 J. Xie, H. Zhang, S. Li, R. Wang, X. Sun, M. Zhou, J. Zhou, X. W. Lou, Y. Xie, *Adv. Mater.,* 2013, **25**, 5807-5813.

48 X-Y. Yu, H. Hu, Y. Wang, H. Chen, X. W. Lou, *Angew. Chem. Int. Ed.* 2015, **54**, 7395-7398.

49. C. Zhang, Z. Wang, Z. Guo, X. W. Lou, *ACS Appl. Mater. Interfaces,* 2012, **4**, 3765-3768.

50 S. Ding, J. S. Chen, X. W. Lou, *Chem. Eur.* J. 2011, **17**, 13142 – 13145.

51 M. A. Lukowski, A. S. Daniel, F. Meng, A. Forticaux, L. Li, S. Jin., *J. Am. Chem. Soc.* 2013, **135**, 10274-10277.

52 D. Hou, W. Zhou, X. Liu, K. Zhou, J. Xie, G. Li, S. Chen, *Electrochimica Acta*, 2015, **166**, 26-31.

53. V. Kiran, D. Mukherjee, R. N. Jenjetia, S. Sampath, *Nanoscale,* 2014, **6**, 12856-12863.

54 N. Pentland, J. O. M. Bockris and E. Sheldon, *J. Electrochem. Soc.,* 1957, **104**, 182.

55 B. E. Conway and B. V. Tilak, *Electrochim. Acta*, 2002, **47**, 3571.

56 J. Deng, W. Yuan, P. Ren, Y. Wang, D. Deng, Z. Zhang, X. Bao, *RSC Adv.,* 2014, **4**, 34733-34738.

57 D. Wang, Z. Wang, C. Wang, P. Zhou, Z. Wu, Z. Liu, *Electrochemistry Communications* 2013, **34**, 219-222

58 Y. Y. Liang, Y. G. Li, H. L. Wang, J. G. Zhou, T. Regies, H. J. Dai, *Nat. Mater.,* 2011, *10*, 780-786.

59 H. Liu, , X. Su, C. Duan, X. Dong, Z. Zhu, *Materials Letters,* 2014**, 122**, 182-185.

60 K. Krishnamoorthy, G. K. Veerasubramani, S. Radhakrishnan, S. J. Kim, *Materials Research Bulletin,* 2014**, 50**, 499-502.

61 Y. Liu, H. Nan, X. Wu, W. Pan, W. Wang, J. Bai, W. Zhao, L. Sun, X. Wang, Z. Ni, *ACS Nano* 2013, **7**, 4202-4209.

62 T. Wang, L. Liu, Z. Zhu, P. Papakonstantinou, J. Hu, H. Liu, M. Li., *Energy. Environ. Sci.,* 2013, **6**, 625–633.

63 H. Vrubel, X. Hu., *ACS Catal.* 2013, **3**, 2002-2011

64 L. Liao , J. Zhu , X. Bian , L. Zhu , M. D. Scanlon , H. H. Girault , and B. Liu., *Adv. Funct. Mater.* 2013, **23**, 5326-5333.

65 Y. Li, H.Wang, L. Xie, Y. Liang, G. Hong, H. Dai, *J. Am. Chem. Soc.,* 2011, **133**, 7296

66 X. Zhao, H. Zhua and X. Yang, *Nanoscale,* 2014, **6**, 10680-10683.

67 J. Xie, J. Zhang, S. Li, F. Grote, X. Zhang, H. Zhang, R. Wang, Y. Lei, B. Pan, Y. Xie, *J. Am. Chem. Soc.,* 2013, **135**, 17881.

68 J. Yang, D. Voiry, S. J. Ahn, D. Kang, A. Y. Kim, M. Chhowalla, H. S. Shin, *Angew. Chem. Int. Ed.* 2013, **52**, 1-5.

69 H. Wang, Z.Lu, D. Kong, J. Sun, T. M. Hymel, Y. Cui, *ACS Nano,* 2014, **8**, 4940-4947.

70 Z. Wu, B. Fang, A. Bonakdarpour, A. Sun, D. P. Wilkinson, D. Wang, *Appl. Catal.,* B, 2012, **125**, 59.

71 S. Muralikrishna, T.N. Ravishankar, T. Ramakrishnappa, D.H. Nagaraju, R. K. Paia, *Environ. Prog. Sustainable Energy,* 2015, DOI: 10.1002/ep.12238.

72 J. D. Benck, T. R. Hellstern, J. Kibsgaard, P. Chakthranont, T. F. Jaramillo, *ACS Catal.* 2014, **4**, 3957-3971.

73. X. Zouc, Y. Zhang, *Chem. Soc. Rev.,* 2015, **44**, 5148-5180.

74 D. Y. Chung, S. K. Park, Y. H. Chung, S. H. Yu, D. H. Lim, N. Jung, H. C. Ham, H. Y. Park, Y. Piao, S. J. Yoo and Y. E. Sung, *Nanoscale*, 2014, **6**, 2131-2136.

75 D. Kong, H. Wang, J. Cha, M. Pasta, K. Koski, J. Yao, Y. Cui, *Nano Letters.,* 2013, **13** 1341–1347.

76 Y. Yan, B. Xia, X. Qi, H. Wang, R. Xu, J-Y. Wang, H. Zhang, X. Wang, *Chem. Commun.,* 2013, **49**, 4884-4886.

77 Y. Zhao, X. Xie, J. Zhang, H. Liu, H-J. Ahn, K. Sun, G. Wang, *Chem. Eur. J.* 2015, **21**, 1-6.

Graphical abstract